Edited by Xiangyu Hu

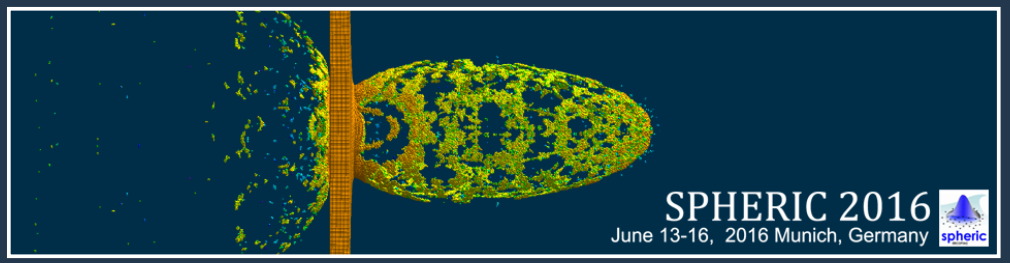

Proceedings of the 11th International SPHERIC Workshop

ISBN 9783000533587

Proceedings of the 11th International SPHERIC Workshop

Edited by Xiangyu Hu

Proceedings of the 11th International SPHERIC Workshop

June 13-16, 2016
TUM, Munich, Germany

ISBN 9783000533587

Organised by

The Institute of Aerodynamics and Fluid Mechanics,
Technical University of Munich

Edited by

Xiangyu Hu

Acknowledgement

The organisers would like to thank

SPHERIC
ERCOFTAC
ALTAIR
NVIDIA
DFG

SPH formulation of the Finite-Time Lyapunov Exponents for the detection of Lagrangian Coherent Structures

P.N. Sun
College of Shipbuilding Engineering
Harbin Engineering University
Harbin, China
sunpengnan@hrbeu.edu.cn

A. Colagrossi, S. Marrone
CNR-INSEAN, Marine Technology Research Institute
Rome, Italy
andrea.colagrossi@cnr.it
salvatore.marrone@cnr.it

A.M. Zhang
College of Shipbuilding Engineering
Harbin Engineering University
Harbin, China
zhangaman@hrbeu.edu.cn

***Abstract*—In the present work, SPH formulae of the Finite-Time Lyapunov Exponents for the detection of Lagrangian Coherent Structures are presented for the analysis of vortical flows with violent fluid material transportation, exchanging and mixing. The Lagrangian Coherent Structures, detected by the ridges of FTLE field, reveal the hidden impenetrable inner boundaries inside the flow, which supplies a useful way for revealing the features e.g. vortices, flow trends etc. especially when moving, deforming or breaking boundaries exist. Thanks to the Lagrangian characteristic of SPH, the trajectory of each fluid particle is explicitly tracked over the whole simulation, which allows for a direct evaluation of the FTLE field implemented during the runtime or conducted as a post-processing. In this paper, δ-SPH method is applied for the numerical simulation and a particle splitting technique is adopted to improve the local accuracy and reduce the total amount of computation. With the scalar fields of FTLE, some representative complex free surface flows with strong vortical motions in naval and ocean engineering are analysis in the section of numerical results. Especially in the last case, the submerged vortical tunnels induced by the splashing bow wave are successfully captured using the proposed method.**

I. INTRODUCTION

When considering a complex flow field, the use of the primary variables (e.g. pressure, velocity, etc.) to analyze the flow features can be not enough. This applies a fortiori especially when treating three-dimensional viscous flows where wakes shed by solid objects are involved. To overcome this limit secondary derived quantities are used in the literature to detect Coherent Structures (CSs), which partition the flow based on the instantaneous distribution of a scalar field, such as: vorticity, Q-criterion [1], Δ-criterion [2], λ_2-criterion [3], etc. These variables are defined mainly based on the instantaneous velocity gradient tensor. However, the advection property of the flow (material transport, exchanging and mixing) cannot be revealed effectively with these definitions. In addition, as stated in Haller [4], under certain conditions most of the definitions of a vortex cannot be objective or not so suitable for an analysis of the flow-data (especially in a 3D context).

The Lagrangian approaches to the CSs are related to the advection of the passive tracers in a finite time interval and therefore it supplies a new way for analyzing and understanding the transport property behind the instantaneous velocity data. Recently a so-called Lagrangian Coherent Structures (LCSs) defined as skeletons of the most repelling or attracting material surfaces (see e.g. [5, 6]) are applied for the flow-data analysis. The LCSs act as inner boundaries that organize the flow trend of the rest fluid material and they clearly show up the flow features like: vortex motions, material transportation, exchanging and mixing, etc., supplying a practical way to explore and understand the underlying mechanisms.

Finite-time Lyapunov Exponent (FTLE) is an objective diagnostic quantity applied by Haller (see e.g. [7, 8]) to detect LCSs. FTLE measures the rate of separation of the nearby fluid particles over a finite time interval. In the forward-time, the ridges (i.e. hypersurfaces along which the variation of the quantity is smaller than transverse to them [6]) of the FTLE scalar field visualize the most repelling material surfaces; conversely in backward-time, the FTLE ridges reveal the most attracting ones. These previously mentioned most repelling or attracting material surfaces constitute the boundaries of the repelling or attracting LCSs.

The main advantages of the FTLE with respect to other quantities as vorticity, Q-surfaces, λ_2-surfaces, etc. can be summarized in:

(i) FTLE is a quantity integrated in time and therefore local fluctuations of the velocity field do not induce much numerical noise on it.

(ii) FTLE is formulated in the Lagrangian framework allowing for a better identification of the LCSs with respect to quantities derived from the velocity gradient.

(iii) The locations of the LCSs are independent of user-defined threshold in a FTLE field while for Eulerian coherent structures, the size and shape change a lot for different quantity thresholds.

(iv) FTLE is able to identify LCSs with an accuracy that in some cases resemble the one obtained by using advanced experimental technique.

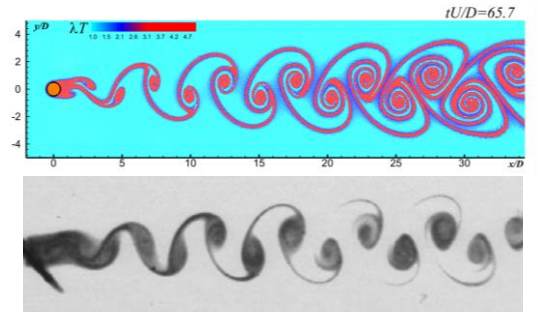

Figure 1. Viscous flow past a circular cylinder at Re = 100. Top: attracting FTLE contour plot through an SPH simulation. Bottom: experimental visualization by Zdravkovich [9].

Top plot of Figure 1 shows an example of the use of attracting FTLE contour plot for capturing the attracting LCSs of a von Karman street shed by a flow past a circular cylinder at Re = 100. The SPH FTLE field has been calculated with the algorithm proposed in Section Ⅲ. On the bottom plot of the same figure a photo from experiments conducted by Zdravkovich [9] is depicted. One may find that the shape of the attracting LCSs resemble the experimental smoke lines. Moreover, the flow structure in the vortex is shown up more clearly by using FTLE than using the smoke line visualization in the experiment.

The present work is dedicated to explain the algorithm for the detection of LCSs in viscous flows through Finite-Time Lyapunov Exponents (FTLEs). A novel numerical technique is presented for the evaluation of the FTLEs in the context of the SPH models. Thanks to the Lagrangian characteristic of SPH, the trajectory of each fluid particle is explicitly tracked over the whole simulation. This allows for a direct evaluation of the FTLE field supplying a new way for the analysis of the scattered flow-data in SPH.

Problems arise in the cases with inflow and outflow boundaries that the particles flowing out on the outflow boundary will be reused again on the inflow boundary, which makes the FTLE calculation in trouble. Therefore, we propose a treatment to update the particle information for the reused particles in the inflow buffer to overcome this problem. In addition, in order to improve the accuracy in some local regions while save the total computational effort, a particle splitting method is also applied, which shows that the present FTLE algorithm is applicable for the simulations with multi-resolutions.

This paper is arranged as follows: in Section Ⅱ, basic principles of FTLE are described; Section Ⅲ is dedicated to the evaluation of FTLE within the SPH framework. Section Ⅳ briefly recalls the SPH scheme used in the present study. Finally, in Section Ⅴ FTLEs are applied to detect the repelling or attracting LCSs in specific numerical test cases. It is demonstrated that FTLEs are fairly suitable in SPH to reveal the main flow features. Conclusions and further development will wrap up the paper.

II. DEFINITION OF THE FINITE TIME LYAPUNOV EXPONENTS IN CONTINUUM MECHANICS

A. *Brief recall of continuum mechanics fundamental concepts*

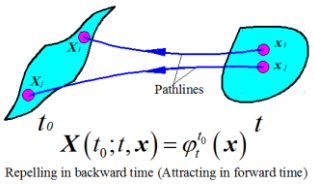

Figure 2. Sketch of the repelling motions of material points in backward time.

In the present section the theory of continuum mechanics is considered in order to define the deformation of elementary fluid volumes when evolving through a flow field. With the flow map ϕ, we have

$$\boldsymbol{x}(t;t_0,\boldsymbol{X})=\phi_{t_0}^{t}(\boldsymbol{X}) \tag{1}$$

The position $\boldsymbol{x}$ at time t of a generic material point is linked to a spatial position $\boldsymbol{X}$ at a past time $t_0 < t$. Due to the properties of the flow map, this function can always be reversed, so that the flow map in the backward time $t \to t_0$ becomes:

$$\boldsymbol{X}(t_0;t,\boldsymbol{x})=\varphi_t^{t_0}(\boldsymbol{x})=\left[\phi_{t_0}^{t}(\boldsymbol{x})\right]^{-1} \tag{2}$$

As depicted in Figure 2, the material points attracting in the forward time $t_0 \to t$ equates to a repelling motion in the backward time $t \to t_0$.

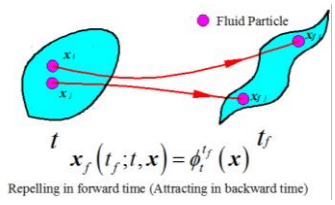

Figure 3. Sketch of the repelling motions of material points in forward time.

Besides the configurations at the past time t_0 and the present time t, for the following analysis, we introduce also a future time configuration at $t_f > t$ with positions $\boldsymbol{x}_f$. Using the map ϕ we get that:

$$\boldsymbol{x}_f(t_f;t,\boldsymbol{x})=\phi_t^{t_f}(\boldsymbol{x}) \tag{3}$$

As depicted in Figure 3, the material points are repelling during the forward time $t \to t_f$. In order to identify univocally the repelling or attracting pathline configurations, the deformation gradient $\boldsymbol{F}$ is defined as:

$$\boldsymbol{F}_{t_0}^{t}(\boldsymbol{X})=\frac{\partial \boldsymbol{x}}{\partial \boldsymbol{X}}=\frac{\partial \phi_{t_0}^{t}(\boldsymbol{X})}{\partial \boldsymbol{X}} \tag{4}$$

The first property of this tensor can be derived through its determinant. Indeed this Jacobian measures the ratio between the elementary volumes dV_0 at times t_0 and dV at time t related to the material point having a past position $\boldsymbol{X}$:

$$J = \det \boldsymbol{F}_{t_0}^{t}\left(\boldsymbol{X}\right) = \frac{dV}{dV_0} \tag{5}$$

If the flow map ϕ describes an incompressible flow, J is always equal to 1 for each time t and for each material point (i.e. $\forall \boldsymbol{X}$).

The so-called forward-in-time Right-Cauchy–Green strain tensor can be evaluated through the relation:

$$\boldsymbol{C}_{t_0}^{t}\left(\boldsymbol{X}\right) = \left[\boldsymbol{F}_{t_0}^{t}\left(\boldsymbol{X}\right)\right]^{T} \boldsymbol{F}_{t_0}^{t}\left(\boldsymbol{X}\right) \tag{6}$$

being $[\,]^T$ the transpose operation. The determinant of $\boldsymbol{C}$ is equal to J^2. In a similar way the above equations can be used to define forward-in-time tensors using the configuration $\boldsymbol{x}$ and $\boldsymbol{x}_f$ at time t and t_f :

$$\boldsymbol{C}_{t}^{t_f}\left(\boldsymbol{x}\right) = \left[\boldsymbol{F}_{t}^{t_f}\left(\boldsymbol{x}\right)\right]^{T} \boldsymbol{F}_{t}^{t_f}\left(\boldsymbol{x}\right) \tag{7}$$

B. Polar decomposition

In order to better understand the physical meaning of the tensors $\boldsymbol{C}$, the polar decomposition of the tensor $\boldsymbol{F}$ is used in the following. The latter consists in the definition of two new tensors $\boldsymbol{R}$ and $\boldsymbol{U}$ such that:

$$\boldsymbol{F} = \boldsymbol{R}\cdot\boldsymbol{U} \quad \boldsymbol{R} \in \mathrm{Orth} \quad \boldsymbol{U} \in \mathrm{Sym} \tag{8}$$

being $\boldsymbol{R}$ the rotating tensor, $\boldsymbol{U}$ the right stretching tensor, Orth the set of the rotation tensors and Sym the set of the symmetric tensors.

Using Eq. (8) on the definition of the Right-Cauchy–Green strain tensor (6) together with the properties of the tensor $\boldsymbol{R}$ and $\boldsymbol{U}$ we get:

$$\boldsymbol{C} = \boldsymbol{F}^{T}\boldsymbol{F} = \boldsymbol{U}^{T}\boldsymbol{R}^{T}\boldsymbol{R}\cdot\boldsymbol{U} = \boldsymbol{U}^{2} \tag{9}$$

Therefore the tensor $\boldsymbol{C}$ is linked just to the stretching deformation of the fluid elementary volumes. From Eq. (9) results that the tensor $\boldsymbol{C}$ is symmetric (like $\boldsymbol{U}$) and positive defined (i.e. $\boldsymbol{C} \in$ Sym+) therefore its eigenvalues are always positive real numbers. The multiplication of the three eigenvalues (in a 3D framework) of $\boldsymbol{C}$ gives:

$$\Lambda_{M\,\mathrm{in}}\Lambda_{2}\Lambda_{Max} = \det\boldsymbol{C} = J^{2} \tag{10}$$

being Λ_{Min} and Λ_{Max} the smallest and largest eigenvalues of the tensor $\boldsymbol{C}$, respectively. If an incompressible flow is considered the above relation becomes:

$$\Lambda_{M\,\mathrm{in}}\Lambda_{2}\Lambda_{Max} = 1 \tag{11}$$

Therefore Λ_{Max} is always a number greater than or equal to 1 measuring an elongation of the fluid volume in the specific direction identified by the related eigenvector. Similarly Λ_{Min} is always less than or equal to 1 measuring the contraction of the fluid volume.

C. Evaluation of the FTLE

Thanks to the above properties the forward-in-time FTLE(+), $\lambda_t^{t_f}$ in the time range $\left(t, t_f\right)$ can be evaluated as

$$\boxed{FTLE^{(+)}} \begin{cases} \lambda_t^{t_f}\left(\boldsymbol{x}\right) = \dfrac{1}{\left|t - t_f\right|}\ln\sqrt{\Lambda_{\max}\left[C_t^{t_f}\left(\boldsymbol{x}\right)\right]} \\ \boldsymbol{C}_t^{t_f}\left(\boldsymbol{x}\right) = \left[\boldsymbol{F}_t^{t_f}\left(\boldsymbol{x}\right)\right]^{T}\boldsymbol{F}_t^{t_f}\left(\boldsymbol{x}\right) \end{cases} \tag{12}$$

The physical meaning of $\lambda_t^{t_f}\left(\boldsymbol{x}\right)$ is the rate of separation of the trajectories of nearby material points in the present reference positions $\boldsymbol{x}$ when moving backward in time $t \to t_f$.

Conversely, using the backward-in-time deformation gradient $\boldsymbol{F}_t^{t_0}$ and the related backward-in-time Right-Cauchy–Green $\boldsymbol{C}_t^{t_0}$, a backward-in-time FTLE(-) $\lambda_t^{t_0}\left(\boldsymbol{x}\right)$ in the time range $\left(t, t_0\right)$ can be evaluated through:

$$\boxed{FTLE^{(-)}} \begin{cases} \lambda_t^{t_0}\left(\boldsymbol{x}\right) = \dfrac{1}{\left|t - t_0\right|}\ln\sqrt{\Lambda_{\max}\left[C_t^{t_0}\left(\boldsymbol{x}\right)\right]} \\ \boldsymbol{C}_t^{t_0}\left(\boldsymbol{x}\right) = \left[\boldsymbol{F}_t^{t_0}\left(\boldsymbol{x}\right)\right]^{T}\boldsymbol{F}_t^{t_0}\left(\boldsymbol{x}\right) \end{cases} \tag{13}$$

The physical meaning of $\lambda_t^{t_0}\left(\boldsymbol{x}\right)$ is the rate of separation of the trajectories of nearby material points in the present reference positions $\boldsymbol{x}$ when moving backward in time $t \to t_0$.

Eqs. (12) and (13) are the key points for the identification of the LCSs as already shown and discussed in the recent literature [5]. Thanks to the use of a future and a past configuration references, both FTLE(+) and the FTLE(−) have been defined on the material points $\boldsymbol{x}$ at the time t .

III. Evaluation of the Lyapunov exponents within the SPH framework

A. SPH approximation formulae

In the SPH method, the spatial derivatives of the primary variables (i.e. velocity $\boldsymbol{u}$ and pressure p) are evaluated through the formulae:

$$\begin{cases} <\nabla\boldsymbol{u}>_i = \sum_j\left(\boldsymbol{u}_j - \boldsymbol{u}_i\right)\otimes\nabla W(\left|\boldsymbol{x}_j - \boldsymbol{x}_i\right|;h)\Delta V_j \\ <\nabla p>_i = \sum_j\left(p_j + p_i\right)\nabla W(\left|\boldsymbol{x}_j - \boldsymbol{x}_i\right|;h)\Delta V_j \end{cases} \tag{14}$$

where ΔV_j is the volume of particle j and $W(\left|\boldsymbol{x}_j - \boldsymbol{x}_i\right|;h)$ is a kernel function with a finite support. The smoothing length h is a reference length of its support. When h goes to zero the kernel function W tends to be a delta Dirac function. For the ease of notation, hereinafter we denote the kernel simply

through W_{ij}. In this work a Wendland C2 kernel function is used with a compact support with a radius equal to $2h$ which remains constant in space and time. The ratio $h/\Delta x$ is set equal to 2, corresponding to a number of interacting neighbours equal to 50 in a 2D framework.

For secondary variables f a more accurate interpolation can be used, for example in this work the following formula is adopted:

$$\begin{cases} <\nabla f(\boldsymbol{x}_i)>=\sum_j\left(f_j-f_i\right)\boldsymbol{L}_i\nabla_i W_{ij}\Delta V_j \\ \boldsymbol{L}_i=\left[\sum_j\left(x_j-x_i\right)\otimes\nabla_i W_{ij}\Delta V_j\right]^{-1} \end{cases} \tag{15}$$

which guarantees the first order completeness (see e.g [10]).

B. SPH evaluation of the FTLE

The proposed method for the evaluation of the FTLE is based on the calculation of the deformation gradient using the sets of the fluid particles $\boldsymbol{X}$, $\boldsymbol{x}$ and $\boldsymbol{x}_f$. The tensor $\boldsymbol{F}$ can be discretized using the formulae presented in the previous section:

$$\begin{cases} \left\langle \boldsymbol{F}_{t_0}^{t}(\boldsymbol{X}_i)\right\rangle=\sum_j\left(\boldsymbol{x}_j-\boldsymbol{x}_i\right)\boldsymbol{L}(\boldsymbol{X}_i)\nabla_i W(\left|\boldsymbol{X}_j-\boldsymbol{X}_i\right|;h)\Delta V_j \\ \boldsymbol{L}(\boldsymbol{X}_i)=\left[\left(\boldsymbol{X}_j-\boldsymbol{X}_i\right)\otimes\nabla_i W(\left|\boldsymbol{X}_j-\boldsymbol{X}_i\right|;h)\Delta V_j\right]^{-1} \end{cases} \tag{16}$$

For the deformation tensor in the forward time $t\to t_f$, a similar equation is given as follows:

$$\begin{cases} \left\langle \boldsymbol{F}_{t}^{t_f}(\boldsymbol{x}_i)\right\rangle=\sum_j\left(\boldsymbol{x}_{fj}-\boldsymbol{x}_{fi}\right)\boldsymbol{L}(\boldsymbol{x}_i)\nabla_i W_{ij}\Delta V_j \\ \boldsymbol{L}(\boldsymbol{x}_i)=\left[\left(\boldsymbol{x}_j-\boldsymbol{x}_i\right)\otimes\nabla_i W_{ij}\Delta V_j\right]^{-1} \end{cases} \tag{17}$$

Regarding the backward-in-time deformation gradient, this can be evaluated as:

$$\left\langle \boldsymbol{F}_{t}^{t_0}(\boldsymbol{x}_i)\right\rangle=\sum_j\left(\boldsymbol{X}_j-\boldsymbol{X}_i\right)\boldsymbol{L}(\boldsymbol{x}_i)\nabla_i W_{ij}\Delta V_j \tag{18}$$

Here the kernel derivation is performed using the particle position $\boldsymbol{x}$ at time t. Both Eqs. (16) and (18) can be implemented in an SPH solver or in a post-processing code giving as inputs the two configurations $\left(\boldsymbol{x}_j,\Delta V_j\right)$ and $\left(\boldsymbol{X}_j,\Delta V_j\right)$ while Eq. (17) can only be evaluated as a post-processing since the particle position $\boldsymbol{x}_f$ is previously unknown.

Substitute Eqs. (17) and (18) into Eqs. (12) and (13) one can evaluate the repelling or attracting FTLE field, in which the ridges constitute the repelling or attracting LCSs [5].

IV. Brief Recall of the Adopted SPH Method

A. δ-SPH scheme

The algorithm proposed in the previous section is applicable for different particle methods, e.g. SPH, MPS etc., since it is simply based on the particle positions at three different time instants:

$$t_0\Rightarrow\left(\boldsymbol{X}_0,\,\Delta V_0\right),\ t\Rightarrow\left(x,\,\Delta V\right),\ t_f\Rightarrow\left(\boldsymbol{x}_f,\Delta V_f\right).$$

In the present work, δ-SPH scheme [11-14] is applied to model some representative complex flows with strong vortical motions in naval and ocean engineering and FTLE is applied to analysis the flow features. A particle shifting technique proposed by Lind et al. [15] is combined with the δ-SPH to reducing the effect of tensile instability. The solid wall boundary is modelled through the use of the fixed ghost particles, see [14].

B. Evaluation of FTLE in presence of inflow and outflow boundaries

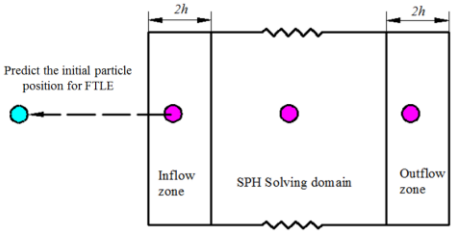

Figure 4 The sketch of the inflow and outflow boundary conditions. When a particle enters the inflow zone, the reference position $\boldsymbol{X}_i$ will be assigned through Eq. (19). The physical variables for particles moving inside the inflow domain and out flow domain are kept constant.

The particles exiting from the outflow boundary will be reused on the inflow zone. For the particles entering the inflow zone, it is needed to update their initial position $\boldsymbol{X}$ with the following equation:

$$\boldsymbol{X}=x-\int_{t_0}^{t}U_{\text{inflow}}(t)\,dt \tag{19}$$

With Eq. (19), we can suppose that the reused particle is the particle starts from $\boldsymbol{X}$ and at time t_0, it reaches the inflow boundary with the velocity $U_{\text{inflow}}(t)$ [5].

C. Evaluation of FTLE in presence of particle spliting technique

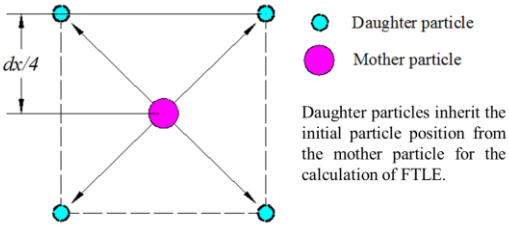

Figure 5. The arrangement for the daughter particles when a mother particle is split.

This part is dedicated to introduce the particle splitting technique allowing for a relatively high particle resolution in the local region of interest and reducing the total computational effort. The algorithm is when a mother particle enters the

splitting region, it is split into four daughter particles on the four vertices of a square centred on the mother one, see the sketch in Figure 5. For the daughter particles, except the mass and volume which are a quarter of the mother ones respectively, they inherit all the other general variables (density, velocity, smoothing length, etc.). It is worth noting that the reference particle positions needed for the FTLE evaluation is also inherited. Since on both sides of the splitting interface, we allow for an identical smoothing length, the SPH approximation there is still accurate and stable, even when particles are split on the free surface.

V. NUMERICAL RESULTS

A. *Flow a past fixed cylinder in a rectangualr box*

The first test-case concerns an ellipse with axis ratio 0.4 moving forward with angle of attack α = 20 in a viscous fluid inside a rectangular box. The rectangular box is $40c$ long and $5c$ wide where c is the major axis of the ellipse. After a short-time acceleration, the ellipse is moving in straight line with a constant velocity U. The Reynolds number of the problem is $Re = Uc/\nu = 500$. No-slip boundary condition is applied on the ellipse while simple free-slip boundary condition is applied on the rectangular wall. The fluid domain is discretized with the resolution $c/\Delta x = 150$ in order to accurately resolve the boundary layer region. An overall number of 4,500,000 particles is used.

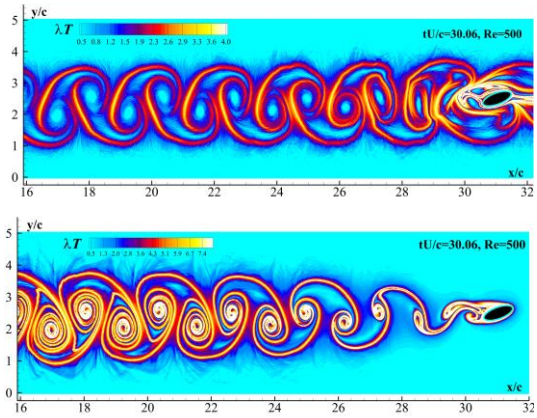

Figure 6. The repelling and attracting LCSs detected by the ridges of the forward time FTLE(+) and backward time FTLE(-) using Eq. (12) and Eq. (13) respectively.

In order to show the most repelling and attracting LCSs in the flow field, Eq. (12) and Eq. (13) is applied to evaluate the backward time FTLE(-) and forward time FTLE(+) respectively in which three different time instants are used: the initial time t_0, a genetic t and the future time $t_f = 40c/U$ seconds. Both FTLE(+) and FTLE(−) are evaluated as a function of the particle positions x_i. In all the results presented the Lyapunov exponent is made non-dimensional using the time range $T = |t_0 - t|$ for the FTLE(−) and $T = |t_f - t|$ for the FTLE(+). For the sake of the simplicity both FTLE(−) and FTLE(+) are indicated with λT in the figure.

In Figure 6, the two different λT fields at time tU/c=30.06 give the loci for the most repelling and attracting LCSs respectively. On the top figure, the positions where the fluid material is subjected to the most stretching deformation is revealed with higher λT, while on the bottom one, higher λT shows the material subjected to strongest attracting deformation. The ridges of the FTLE(+) and FTLE(−) distribution construct the repelling and attracting LCSs respectively.

It is worth noting that the backward time FTLE(−) reflects the shedding of a classical von Karman Vortex Street and it resembles the one obtained with numerical streaklines by [16].

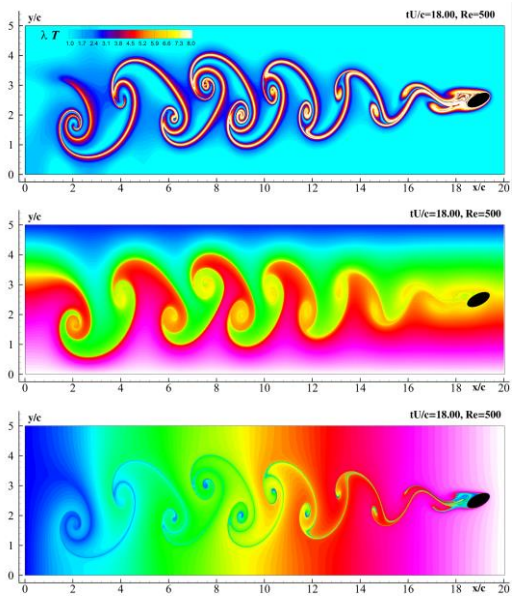

Figure 7. The plots of the Lagrangian tracers at time $tU/c = 18$ according to their initial vertical coordinates.

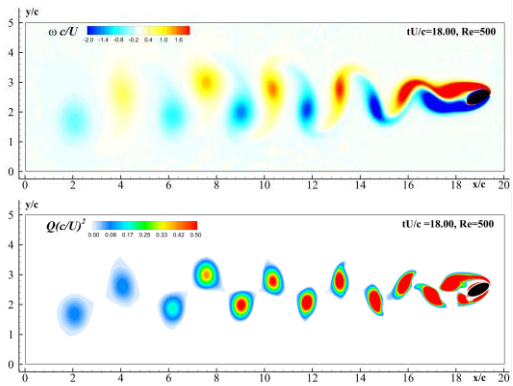

Figure 8. Viscous wake shed by a moving inclined ellipse: vorticity field (top) and second invariant of the velocity gradient Q (bottom) at time $tU/c = 18$.

Based on the same case, we distribute some Lagrangian tracers at the beginning of the simulation and plot them at $tU/c = 18$ according to their initial vertical and horizontal coordinates. Compare the top and middle plots in Figure 7, we can find that attracting LCSs have the same shape of the inner

boundaries for the fluid material transportation, which means that with attracting LCSs, the flow field is partitioned into several parts and the flow cannot penetrate the boundaries of these regions. However, through the bottom plot which is contoured according to the initial horizontal coordinates of the tracers, one can only observe the fluid material transportation in the horizontal direction. That means using the Lagrangian tracers, the physical phenomena is observed dependent on how the tracers are plotted, but with attracting FTLE$^{(-)}$, inner flow boundaries are revealed independent from the user effects. Therefore one can see clearly how the fluid material is transported or mixed after the elliptical cylinder passes in the rectangular box.

The following part is dedicated to show the vortex structure revealed by the FTLE$^{(-)}$ ridges. Usually the vortex structure is shown by the Eulerian defined quantities. Here we plot the vorticity and second invariant of the velocity gradient Q in Figure 8. Compare Figure 7 and Figure 8, one may find that the whirling parts of the attracting LCSs locate the boundaries of the vortices shed from the ellipse. In addition, the flow structure inside the vortices is also shown clearly. However, by the vorticity or Q-definition, the information inside the cortex is hidden. Furthermore, the region of the vortex is also dependent by the artificial chosen threshold of the quantities as already emphasized. Considering the advantages of the FTLE$^{(-)}$ ridges in showing up the flow features, FTLE$^{(-)}$ is the main topic hereinafter.

B. Rotating and sinking of a rectangular box

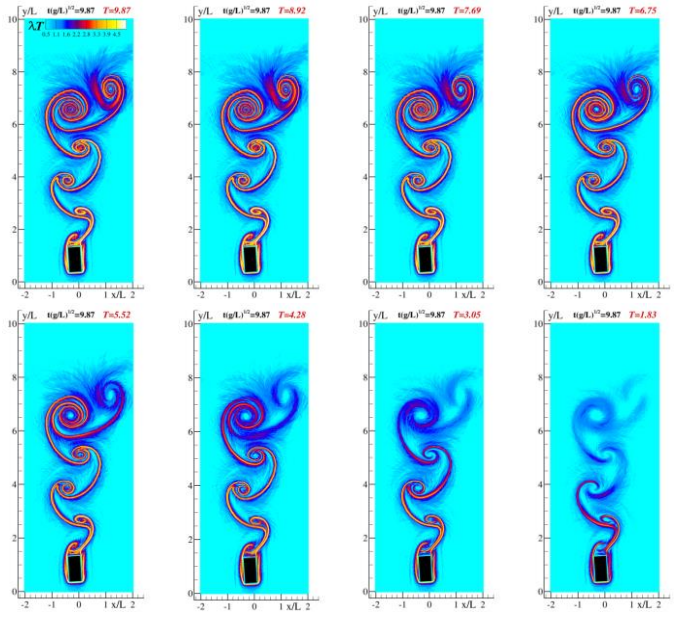

Figure 9 The attracting LCSs detected with different time interval T .

In the calculation of FTLE, the magnitude of the time interval T is less discussed in the literature. In this part, based on the case of the rotating and sinking of a rectangular box with the length of L and width of $0.5L$, we investigate the effect of T on the distribution of the backward time FTLE$^{(-)}$. In the setup of the present simulation, the density of the rectangular box is twice as the one of the fluid. The box center is horizontally located at $(0.5L, 7.5L)$ initially. The gravity center of the box is shifted by $0.25L$ from the box center to the right side. On the rectangular box, no-slip boundary condition is applied while on the outside boundary which is $4L$ wide and $10L$ high, simple free-slip boundary condition is applied.

Due to the density difference, after the release, the box starts to rotate and sink. Finally, at $t\left(g/L\right)^{1/2} = 9.87$, the box is about to touch the bottom. The backward time FTLE$^{(-)}$ field is calculated using Eq. (13) with different time interval T, which is decreasing gradually from left to right and top to bottom, as is shown in Figure 9. When T is larger than 6.75, the distributions of the LCSs are similar. That means increasing the time interval makes negligible effects on the shape of the LCSs. However, when the time interval is decreased, it is found that the vortex structures at the end of the LCSs are gradually lost. Finally, when $T = 1.83$ is used, there remains very few vorticities close to the box. The reason is when a small time interval is used, the fluid deformations before the reference time t_0 are lost. However, even the time interval is changed; the shape of the LCSs remains similar. That means the detection of the LCSs with FTLE is free from the user-defined threshold of the time interval T . Nevertheless a large time interval is necessary to reveal complete LCSs inside the whole flow field. Therefore in the present work, we use the initial fluid configuration as the reference one, i.e. using $T = t_{present}$ for FTLE$^{(-)}$.

C. Flow past an ellipse beneath a free surface

In this part, the flow past an elliptical cylinder beneath a free surface is numerically investigated. The axis ratio of the ellipse is 0.4 and it is placed at $x = 0, y = 0$ with the angle of attack $\alpha = 20$. The inflow boundary is positioned at $x/c = -6$ and outflow one at $x/c = 24$. The undisturbed fluid surface lies at $y/c = 1$ and the fluid bottom lies at $y/c = -5$. In order to reduce the total amount of calculation, the particle splitting technique introduced in Section Ⅳ is applied. For the fluid particles flowing after $x/c = -1.5$ and $y/c > -2$, it is split into four daughter particles.

The distributions of the attracting LCSs (ridges of FTLE$^{(-)}$) at different time instants are shown in Figure 10. Near the cylinder, in the region $x/c < 5$, the vortex street is still similar to the traditional Karman Vortex Street. However, as the wake propagates further and expands in the vertical direction, the free surface yields a repelling effect on the vortices, which finally pair forming a horizontal pattern (see in the region $x/c > 5$). Furthermore, because the fast current originated above the elliptical cylinder, plunging breakings are forced in the upstream direction and some vortex structures are created, see the figures at $t(g/c)^{1/2} = 6.48$ and $t(g/c)^{1/2} = 9.72$

in Figure 10. At $t(g/c)^{1/2} = 12.96$, these vortex structures originated from the breaking surface are absorbed by the underlying von Karman street because of their downward motions. Finally at $t(g/c)^{1/2} = 18.36$, the flow reaches a steady stage. The attracting LCSs show up the inner boundaries of the fluid material transportations. In the region of $x/c > 10$, some part of the LCSs touches the free surface, that means as the fluid flow past the ellipse, the deeper fluid is gradually transported to the fluid surface and the fluid material initially on the surface is carried downward by shed the vortices.

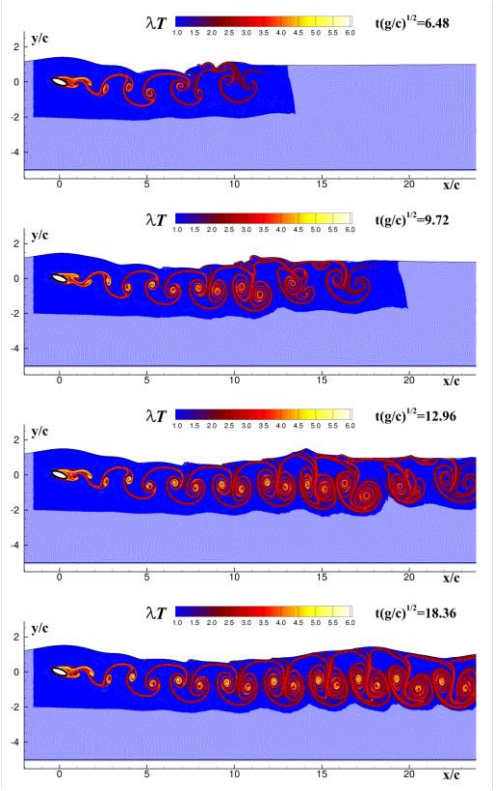

Figure 10. Flow past an elliptical cylinder beneath a free surface: FTLE$^{(-)}$ contour plots for four different time instants showing the interaction between the Karman vortex street and the free surface.

For such a case FTLEs supply an effective way to reveal these vortex structures, the material exchanging between the surface fluid and deeper one and show the interesting process of the interactions between vortices and the free surface.

D. Breaking wave pattern generated by fast ships

The last test case studied is the breaking and splashing of bow waves for high speed ships. In order to make this case easier for the readers to reproduce, we adopt a simplified ship configuration as shown in Figure 11.

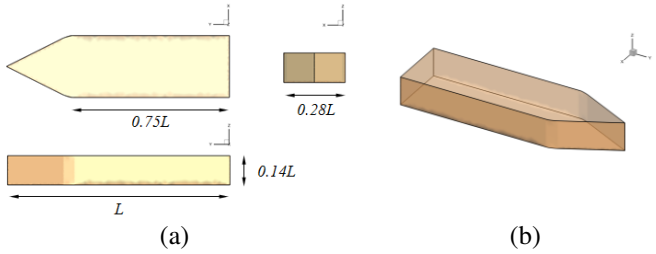

Figure 11. (a) The three view drawing for the simplified ship model; (b) the pictorial drawing of the simplified ship model.

In [17] the breaking wave pattern of a fast ship has been studied in detail for different forward ship speeds. In that work a 2D + t SPH model has been used and the vortical structures due to plunging of the bow wave are tracked using passive markers initially positioned on the undisturbed free surface. The same technique has been also adopted in [18] combining with vorticity contour plots. In the present work a similar case is conducted to show the benefits of using the FTLEs for capturing the bow breaking wave features. In this section the FTLE$^{(-)}$ is calculated to detect the submerged vortical tunnels entrapped by the breaking phenomena. In this study, the water depth of the fluid domain is 5 times deeper than the ship draught, which avoids the shallow water effects.

This test-case is an attempt to extend the detection of LCSs from a 2D to a 3D framework and to show its potential application in naval engineering. The ship Froude number considered is $Fr = U/\sqrt{gL} = 0.41$ with L is the ship length and U the forward ship speed. For this case an intense plunging breaking is generated by the bow wave with the entrapment of two vortex tubes running along the whole ship length.

Top plot of Figure 12 depicts a panorama view of the simplified ship. The particle belonging to the free surface are identified through the algorithm presented in [19] and plotted in blue. The other particles are plotted with a colour contour plot of the FTLE$^{(-)}$ indicated with λT. Only the particles having a λT larger than 2, which detect the LCSs related to the two submerged vortex tubes, are plotted. This clearly shows that through the FTLE$^{(-)}$ it is possible to reduce the amount of data for representing the LCSs, which is a remarkable advantage for the analysis and for the storing of 3D data. In middle plot of Figure 12 a detail of the flow in the bow region is depicted. Two submerged vortex tubes, originated by the first and second plunging jet is shown up by the FTLE$^{(-)}$ plot. In addition, in the downstream of the ship shoulder, another vortex tunnel is generated. This vortex is caused by the sharp corner at the bilge of the simplified ship model. However, for a ship with a round bilge, this vortex is not created, see in [5]. In bottom plot of Figure 12, a rear view from right astern shows the height of the splash-up of the free surface and the depth of entrapped vortex tunnels. The vortex tunnel carries the fluid material from the water surface to the inner region and the vortex boundary reaches even deeper than the draught of the ship. It is highlighted that for fast surface-

piercing ships, the disturbing to the fluid is not only confined to the surface region, but also deep into the water even deeper than the ship draught and FTLE$^{(-)}$ supplies a practical way to reveal the fluid material transportation generated by the entrapped vortices.

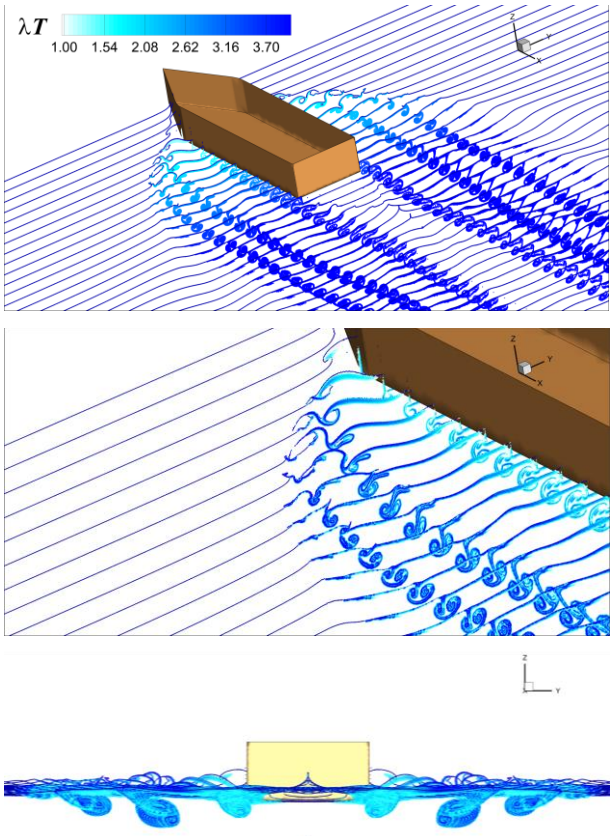

Figure 12. Breaking wave pattern generated by the simplified ship model at $Fr = U/\sqrt{gL} = 0.41$. Top: FTLE$^{(-)}$ contour plots, only particles with λT greater than 2 are plotted. The particles belonging to the free surface are added and plotted in blue. Middle: a detail of the bow wave released from the ship shoulder. Bottom: a rear view from right astern shows that the vortical tunnel reaches even much deeper than the draught of the ship.

VI. CONCLUSION

In this work the Finite-Time Lyapunov Exponents (FTLEs) are formulated in the SPH framework for the detection of Lagrangian Coherent Structures (LCSs). From the continuum mechanics theory and using the Polar Decomposition it is shown that the FTLEs represent a measure of attraction and repulsion of pathlines during the flow evolution. Then, the theory of the Lyapunov Exponents has been introduced in the Smoothed Particle Hydrodynamics context allowing for a direct evaluation of the FTLE fields.

The novel formulations introduced for the FTLEs calculation within the SPH method have been finally tested on four different test-cases of increasing complexity. It is shown that the attracting LCSs revealed by the ridges of FTLE$^{(-)}$ plot gives the boundary of the fluid material transportation and further the vortex positions. The combination of SPH and FTLE is applicable for free surface problems with serious free surface splash-up. Especially for the naval engineering problem the proposed algorithm has been successfully applied to capture the submerged vortical tunnels caused by the splashing bow wave. In future the present technique will be extended to the 3D framework.

ACKNOWLEDGEMENT

This paper is funded by the International Exchange Program of Harbin Engineering University for Innovation-oriented Talents Cultivation. This work is also funded by: CNR-INSEAN within the Project PANdA: PArticle methods for Naval Applications, protocol number N. 3263, 21 October 2014, the China Scholarship Council (CSC), the National Program for Support of Top-notch Young Professionals and the Science Foundation for Young Scholars of Heilongjiang Province (QC2016061).

REFERENCES

[1] H. JCR, A. Wray, P. Moin, Eddies, stream, and convergence zones inturbulent flows, Center for turbulence research report CTR-S88, (1988) 193-208.
[2] M. Chong, A.E. Perry, B. Cantwell, A general classification of three - dimensional flow fields, Physics of Fluids A: Fluid Dynamics (1989-1993), 2 (1990) 765-777.
[3] J. Jeong, F. Hussain, On the identification of a vortex, Journal of fluid mechanics, 285 (1995) 69-94.
[4] G. Haller, An objective definition of a vortex, Journal of fluid mechanics, 525 (2005) 1-26.
[5] P. Sun, A. Colagrossi, S. Marrone, A. Zhang, Detection of Lagrangian Coherent Structures in the SPH framework, Computer Methods in Applied Mechanics and Engineering, (2016).
[6] G. Haller, Lagrangian coherent structures, Annual Review of Fluid Mechanics, 47 (2015) 137-162.
[7] G. Haller, Lagrangian structures and the rate of strain in a partition of two-dimensional turbulence, Physics of Fluids (1994-present), 13 (2001) 3365-3385.
[8] G. Haller, Distinguished material surfaces and coherent structures in three-dimensional fluid flows, Physica D: Nonlinear Phenomena, 149 (2001) 248-277.
[9] M. Zdravkovich, Smoke observations of the formation of a Karman vortex street, Journal of fluid mechanics, 37 (1969) 491-496.
[10] P. Randles, L. Libersky, Smoothed particle hydrodynamics: some recent improvements and applications, Computer Methods in Applied Mechanics and Engineering, 139 (1996) 375-408.
[11] M. Antuono, A. Colagrossi, S. Marrone, C. Lugni, Propagation of gravity waves through an SPH scheme with numerical diffusive terms, Computer Physics Communications, 182 (2011) 866-877.
[12] M. Antuono, A. Colagrossi, S. Marrone, D. Molteni, Free-surface flows solved by means of SPH schemes with numerical diffusive terms, Computer Physics Communications, 181 (2010) 532-549.
[13] M. Antuono, S. Marrone, A. Colagrossi, B. Bouscasse, Energy balance in the δ-SPH scheme, Computer Methods in Applied Mechanics and Engineering, 289 (2015) 209-226.
[14] S. Marrone, M. Antuono, A. Colagrossi, G. Colicchio, D. Le Touzé, G. Graziani, δ-SPH model for simulating violent impact flows, Computer Methods in Applied Mechanics and Engineering, 200 (2011) 1526-1542.
[15] S.J. Lind, R. Xu, P.K. Stansby, B.D. Rogers, Incompressible smoothed particle hydrodynamics for free-surface flows: A generalised diffusion-based algorithm for stability and validations for impulsive flows and propagating waves, Journal of Computational Physics, 231 (2012) 1499-1523.
[16] A. Colagrossi, E. Rossi, S. Marrone, The Discrete Vortex Hydrodynamics method: similarities and differences with the SPH, 10th international SPHERIC workshop Parma, Italy (June, 16-18 2015).
[17] S. Marrone, A. Colagrossi, M. Antuono, C. Lugni, M. Tulin, A 2D+t SPH model to study the breaking wave pattern generated by fast ships, Journal of Fluids and Structures, 27 (2011) 1199-1215.
[18] M. Landrini, A. Colagrossi, M. Greco, M. Tulin, The fluid mechanics of splashing bow waves on ships: A hybrid BEM–SPH analysis, Ocean Engineering, 53 (2012) 111-127.
[19] S. Marrone, A. Colagrossi, D. Le Touzé, G. Graziani, Fast free-surface detection and level-set function definition in SPH solvers, Journal of Computational Physics, 229 (2010) 3652-3663.